Broadband Calibration of E-Field Probes in Lossy Media

Klaus Meier, Michael Burkhardt, Thomas Schmid, and Niels Kuster

Abstract— **A broadband calibration procedure for E-field probes that minimizes the overall uncertainties inherent in E-field measurements in lossy dielectric liquids has been developed. The analysis of the calibration requirements shows that probes that are symmetrical with respect to their axis greatly facilitate accurate calibration, since the calibration procedure can be divided into several discrete steps. Such a procedure is presented and analyzed with respect to its uncertainties. Absolute calibration is performed at three frequency bands utilized in Europe for mobile communications (450 MHz, 900 MHz, and 1.8 GHz) and in different tissue-simulating liquids. The parameters obtained are verified by numerical simulations of the probe in the surrounding media. Such simulations allow the assessment of some of the calibration parameters with sufficient accuracy in cases where the experimental determination would be too tedious and time consuming.**

I. Introduction

IN VIEW OF THE phenomenal growth of the mobile communications market, the telecommunications industry has lately recognized the need to test its mobile telephones for compliance with the safety limits. The current safety limits for the frequency range of mobile communications are defined by the maximum tolerable absorbed power per tissue mass in W/kg, known as the specific absorption rate (SAR). The local SAR can be determined experimentally by measuring either the induced electrical field strength E (RMS value of the Hermitian magnitude) or the temperature rise $\partial T/\partial t$ caused in the tissue by the absorption

$$\begin{aligned} \mathrm{SAR} &= \frac{\sigma}{\rho} E^2 \\ &= c \frac{\partial T}{\partial t} \end{aligned} \tag{1}$$

where σ is the conductivity, ρ is the mass density, and c is the specific heat of the tissue at the site of measurement.

Since measurements using thermal probes do not provide an adequate degree of efficiency and sensitivity for compliance-testing of consumer products, research up until today has been focused on E-field probes inside tissue-simulating media.

The original design of a miniaturized isotropic E-field probe for use in tissue-simulating liquids goes back to Bassen *et al.* [1]. The authors recently presented a new probe design [2], [3] with significantly improved performance characteristics.

Manuscript received October 2, 1995, revised May 1, 1996.

The authors are with the Swiss Federal Institute of Technology (ETH), CH-8092 Zurich, Switzerland.

Publisher Item Identifier S 0018-9480(96)07039-1.

In view of the significance of and difficulties involved in accurate calibration, surprisingly little has been published so far about broadband calibration of isotropic E-field probes in dielectric materials. In [4], a calibration procedure in an S-band waveguide at a single frequency of 2.45 GHz is described. The calibration uncertainties due to the dependence of the probe sensitivity on polarization, frequency, dielectric parameters of the surrounding media, and spatial resolution, however, have only been marginally addressed. If these effects are not carefully considered, the measurements errors can easily be in the range of 3–6 dB or larger. Especially in view of the limited leeway possible with respect to the safety limits of modern telecommunications equipment [5], such uncertainties are not tolerable for dosimetric-type approval setups.

In this paper the error sources that depend on the design of the E-field probes are discussed. Based on these considerations a broadband calibration procedure for the dosimetric probe previously presented in [2] was developed with the objective of minimizing the uncertainties for dosimetric assessment.

II. Calibration Requirements

E-field probes with isotropic response are achieved by the orthogonal positioning of three sensors, each sensitive to one E-field component. Short dipoles or small E-field-sensitive crystals have these characteristics. In miniaturized E-field probes, small dipoles equipped with diode rectifiers are generally used, since they offer the greatest sensitivity and have a linear response over a wide frequency range. Phase information is not required, since SAR is proportional to the Hermitian magnitude. For use in liquid media the sensors must be protected, i.e., encapsulated. This usually affects the performance of the probe considerably.

The probe (SPEAG Model ET3DV4) for which the calibration is demonstrated is shown in Fig. 1. It consists of three small dipoles (3 mm in length) directly loaded with a Schottky diode and connected via resistive lines to the data acquisition electronics. The core that holds the ceramic substrates as well as the outer shell are made of the synthetic microwave material STYCAST0005 with a permittivity of 2.54 and a loss tangent of 0.0005. In its center the optical multifiber line is inserted, enabling contactless surface detection.

The basic requirement for calibration is that the output signals of three orthogonally positioned sensors be evaluated in such a way that the reading corresponds to the SAR at the measurement site *in the absence of the probe.* Unfortunately,

the relation between the field and the sensor signals depends on several factors:

1) design and construction materials of the probe;
2) electrical properties of the surrounding media;
3) direction and polarization of the field;
4) field gradient at the measurement site;
5) RF characteristics of the antenna, the rectifying element, and the transmission line;
6) higher-order modes or different reception modes in the probe;
7) sensitivity of the rectifier;
8) characteristics of the evaluation circuit for the rectified signals.

The calibration essentially attempts to describe these effects quantitatively, so that correct SAR values can be obtained under various measurement conditions. Furthermore, it is important to know the absolute uncertainty and the validity range of the calibration. the first four factors, however, have scarcely been addressed in previously applied calibration techniques. These factors are briefly discussed in the following.

Influence of the Probe Material on the Field: Any dielectric material around electric dipoles generally alters the local signal strength inside the probe. For probe constructions as shown in Fig. 1 the influence on E-field components normal to the probe axis will be different from that on E-field components parallel to the probe axis. Furthermore, this difference in sensitivity depends on the surrounding medium. This results in poor isotropy in planes that are aligned to the probe axis. For example, a deviation from isotropy of less than 0.2 dB is easily achievable around the probe axis (i.e., E-field polarization normal to the probe axis), owing to symmetry. For E-field polarizations in planes aligned to the probe axis, however, the deviation is larger than 1.5 dB in air and reduces to 0.6 dB in brain equivalent tissue [2]. In [3], several methods are presented to compensate for these effects. In any case, the directivity characteristics of the probe will be different in different media. In addition, these effects are frequency-dependent in lossy media.

Effects in Strongly Nonhomogeneous Fields: Special considerations are needed if the field significantly changes within the probe's dimensions, e.g., at higher frequencies inside lossy material. Therefore, a calibration reference point in the probe is defined. However, the sensor response may depend significantly upon the probe's alignment with respect to the direction of the field gradient. In addition, each field component is measured at slightly different locations, due to the spacing between the sensors. These effects result in an increased deviation of isotropy and must be carefully analyzed.

Influence of Material Discontinuities: In the immediate vicinity of material discontinuities the dielectric body of the probe has a significantly different effect on the field than within homogeneous material. For example, an increase in sensitivity can be observed when the probe approaches the surface of a shell phantom (see also Figs. 5–8). In these cases the calibration performed for homogeneous materials is not valid.

To keep the number of calibration parameters and calibration measurements low, it is crucial to separate the above-listed influences and quantify them individually. Since the calibration is principally valid only for the special conditions under which the calibration has been performed, an analysis of uncertainty must be performed for the conditions under which the probe is actually used. For axis-symmetrical probes it is possible to calibrate the probe in a three-step approach, as shown in the next section. Furthermore, the proposed setups for calibration also closely correspond to those of the dosimetric assessments performed with the scanner, as described in [2].

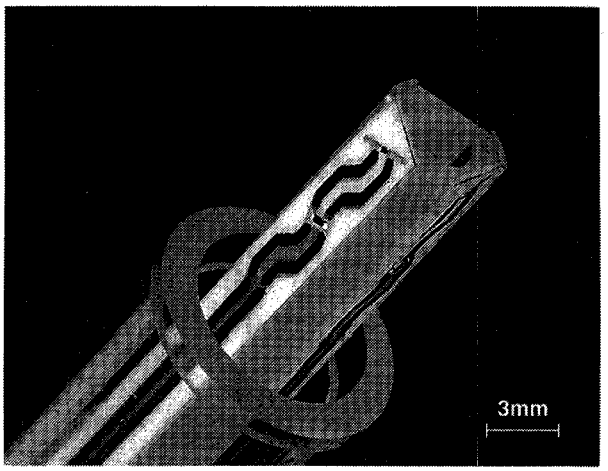

Fig. 1. Tip of the E-field probe. The tip encapsulation has been removed. One 3-mm-long dipole and the diode can be seen. In the center of the core is the opening for a built-in optical proximity sensor.

III. Three-Step Calibration Approach

A three-step approach is possible if the calibration factor can be separated into three independent factors $f_i(V_i)$, η_i, and γ_i

$$|E^2| = \sum_{i=1}^{3} |E_i^2| = \sum_{i=1}^{3} \frac{f_i(V_i)}{\eta_i \gamma_i} \tag{2}$$

where V_i is the rectified signal from the sensor elements.

1) $f_i(V_i)$: In most cases V_i needs to be linearized, because of the nonlinear response of the output dependent on the rectifier (diode compression) and evaluation circuit. This is a function of the magnitude of the rectified signal only and independent of the RF-transmission to the diode. V_i is monitored during a power scan of the exciting field. The linearization function is evaluated, so that $f_i(V_i)$ is proportional to the square of the exciting field strength. When the rectifying elements and evaluation channels are identical, the same function $f[f_i(V_i) = f(V_i)]$ can be used for all sensors. In the case of amplitude-modulated signals, the timing characteristics of the evaluation circuit must also be taken into account. For pulsed signals with a known crest factor, a simple correction formula can be given; for arbitrary modulations, however, a more sophisticated signal analysis is necessary.

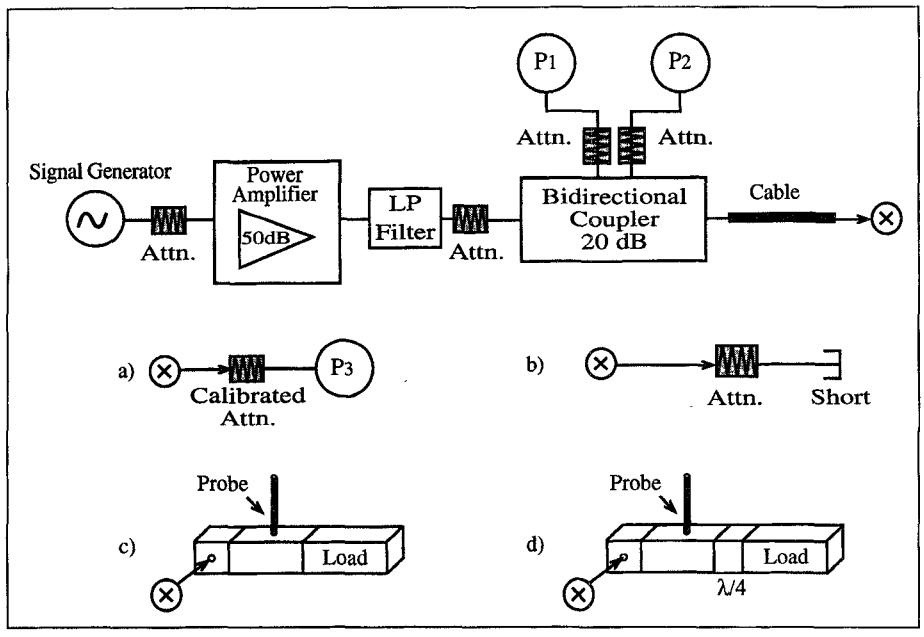

Fig. 2. Setup for calibration in wave guides, i.e., in air. Measurements a and b to calibrate the power meters P_1 and P_2 with respect to the high-precision meter P_3. Probe measurements c and d with different distances to load. By adjusting the amplification to keep P_1 constant, the waveguide input power is equal to the power reading P_3 plus the attenuation of the calibrated attenuator.

2) η_i: These factors describe the relation between the linearized signal of a single sensor $f_i(V_i)$ and the field component in the direction of the sensor [μ V/(V/m)^2] in air. Aside from the dipole length, they depend on the probe's materials, the sensor's positioning, and the RF characteristics of the sensor components. If detector diodes are used as rectifying elements, the parasitic capacitance, which is generally not precisely specified, influences the RF behavior. Therefore, the factors η_i will be different for each sensor, even if the sensors are positioned in a symmetrical fashion. These factors can be assessed by standard probe calibration procedures (see Section IV). All error sources (isotropy, frequency linearity) must be investigated during this calibration in order to assess the calibration factors for an average measurement situation and to evaluate the error and validity range of the calibration. For broadband E-field probes, the calibration factors are independent of the frequency over a wide range (two–three decades) and can thus be considered to be constants.
3) γ_i: These factors describe the ratio of the sensitivity of the probe sensors in different media to their sensitivity in air, i.e., $\gamma_i = 1$ for air. These usually depend both on the surrounding material and the frequency and on the materials and the design of the probe. In other words, the (time-consuming) assessment of these calibration factors (see Sections V and VI) need only be done once for each probe type, and not for each individual probe. It is further necessary to reassess the deviation from isotropy in liquid, since it may differ from air (see Section II). In the case of symmetrical sensor positioning they will in fact be identical for each sensor ($\gamma_i = \gamma$). γ will hereafter be called the "conversion factor."

The separation of the calibration factor in a probe and sensor dependent factor η_i and a probe type and situation-dependent conversion factor γ_i is an approximation that is based on various assumptions:

- The variation of the dipole impedance caused by the surrounding medium is the same for all sensors.
- The local E-field distribution in the area of the sensors inside the probe only depends in magnitude on the surrounding medium. In symmetrical probes this fact can be regarded more leniently.
- The differences (manufacturing tolerances) between probes of the same type are small.

The validity of these assumptions depends largely on the probe's design. Measurements and simulations of our probes have established the feasibility of this calibration procedure. In the following the setups and procedure are described in detail, from which the factors η_i and γ_i have been determined.

IV. Calibration in Air

To calibrate the probe in air, a well-defined measurement volume with a known and largely homogeneous electrical field is necessary. Since reference probes are usually not accurate enough, the field strength must be determined from power measurements. Depending on the frequency, different setups were used to calibrate the probe in air.

1) For frequencies over 1 GHz standard wave guides R22 and R26 were used with the setup according to Fig. 2. The probe was rotated around its axis with a positioning accuracy at the probe tip of better than ± 0.1 mm. By using high-precision components (loads, lines, and adaptors) and error compensation methods, an absolute accuracy of better than $\pm 5\%$ was achieved. The linearity over different frequencies and wave guides is better than

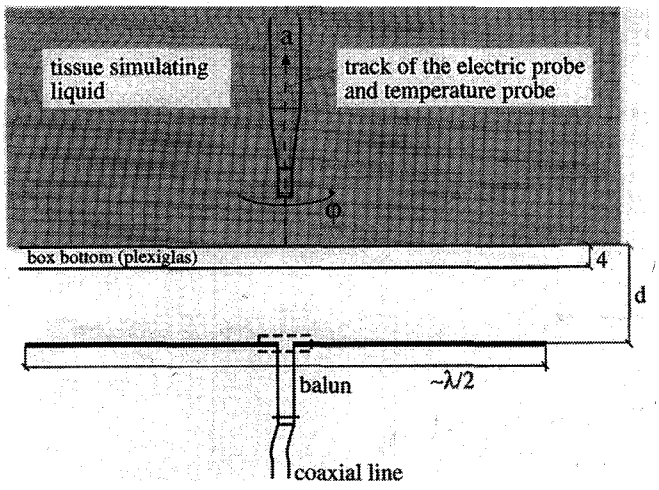

Fig. 3. Experimental setup. On the top is the Plexiglass box filled with the simulating liquid. At the bottom is the dipole. The temperature probes and the E-field probe are positioned directly above the dipole feedpoint.

±2%. The probe produced reflections of 1.6% in the R22 wave guide and of 2% in the R26 wave guide.

2) At frequencies below 1 GHz a TEM cell (ifi110) with rectangular cross section was used. The field gradient at the calibration location in the center over the septum was less than ±2%/cm. By taking into account all error sources in the field calculation an absolute accuracy of not better than 10% can be achieved. However, the agreement with the wave guide measurement was within ±3% and the linearity from 30–900 MHz was within ±2%. Probe reflections were found to be negligible.
3) In the waveguide and TEM-cell measurements, the isotropy around the probe axis can only be assessed. To measure the isotropy in all directions, the following near-field setups were applied. At lower frequencies the field in the symmetry plane of symmetric standard dipoles was used (similar to the setup of Fig. 3). At higher frequencies, the center point over an open waveguide was chosen as the measurement location. These measurement setups permit the assessment of the isotropy in all directions. The same setups can also be used to determine the deviation from isotropy inside different media [2].

V. Experimental Determination of Conversion Factor γ

A. Setup

To determine the conversion factor γ, a well-defined SAR distribution inside the dielectric material for which the probe must be calibrated is needed. The local SAR values can be experimentally measured using small thermal probes according to (1) at high power levels. Furthermore, setups are preferred that allow the computation of the field inside the dielectric material analytically or by numerical simulations. One way would be to use a dielectric slab in a rectangular waveguide. Although the induced fields are well defined and can be easily determined if the emergence of spurious higher modes can be sufficiently suppressed, the setup is very narrow-banded.

Another setup used in [6] is the simulation of a dielectric half-space, which is exposed to a $\lambda/2$ dipole aligned parallel to the surface of this half-space (Fig. 3). For this configuration accurate results can be achieved by computer simulations since the SAR on the axis is largely proportional to the square of the antenna feedpoint current and not to the output power or to the incident E-field, i.e., does not require integrals in closest proximity of the gap. The drawback is that the feedpoint current can only be experimentally assessed with fairly large uncertainties of no better than ±10%.

This setup was nevertheless chosen since:

- it is easy to set up and handle;
- it provides much greater flexibility, since a broad frequency range can be covered by the same setup; and
- it is a good representation of the test situation implemented for dosimetric assessments of mobile communications devices [2].

The half-space was experimentally simulated by an acrylic glass box ($800 \times 600 \times 200$ mm^3) filled with the lossy dielectric liquid. The thickness of the acrylic glass box phantom was 4 mm. The standard dipoles were placed parallel to the dielectric surface at distances that were small compared to the dimensions of the box and to the distance from the floor. The floor was lined with absorbers.

B. Brain-Simulating Liquids

The dielectric data for brain tissue available in literature varies considerably, i.e., up to ±25%, whereby uncertainty and variations of the values for human brain tissue are not given. The basis for our studies was the most recent data for living tissues. In [7], the mean values of grey and white matter at 900 MHz are $\epsilon_r = 43$ and $\sigma = 0.85$ mho/m. In [8], white matter at 450 MHz is determined to have $\epsilon_r = 48$ and $\sigma = 0.6$ mho/m. Liquids that allow the simulation of similar brain parameters at 450 and 900 MHz and which are inexpensive and easy to handle consist of sugar, water, NaCl, and Hydroxyethylcellulosis (HEC) [8], [9]. For brain tissue at 1.8 GHz, two different liquids were used. The first (1800_A) was based on a simple sugar-water solution without any salt (free ions). Nevertheless, the conductivity of such a solution was still higher than the brain tissue parameters in [7] (Table I). For grey matter the corresponding values would be $\epsilon_r = 41$ and $\sigma = 1.45$ mho/m. The reason is that the bound sugar–water complexes begin to determine the conductivity of the liquid at frequencies higher than 1 GHz. Therefore, sugar was replaced by butyldigol (2-(2-butoxyethoxy)ethanolbutyl) which, when dissolved in water, shows smaller conductivity values. At the same ϵ_r value, the conductivity could be reduced from 1.65–1.25 mho/m (1800_B). The mean values for grey and white matter according to [7] are $\epsilon_r = 41$ and $\sigma = 1.15$ mho/m.

The electrical parameters were measured by an open coaxial method using the HP 85070A Dielectric Probe Kit. To verify the open coaxial method, we determined the electrical parameters using the slotted-line method. The agreement was within 4%. Table I gives an overview. The temperature dependence of the liquid's parameter was also checked. In the temperature

TABLE I
DIELECTRIC PROPERTIES AND CONVERSION FACTOR γ OF BRAIN TISSUE-SIMULATING LIQUIDS AT THE TESTED FREQUENCIES OF 450 MHz, 900 MHz, AND 1.8 GHz. AT 1.8 GHz, TWO LIQUIDS WERE USED: (a) SUGAR–WATER SOLUTION. AND (b) BUTYLDIGOL–WATER SOLUTION

f [MHz]	ϵ_r	σ [mho/m]	γ
450	47.0 ± 5%	0.43 ± 6%	6.7 ±10%
900	40.0 ± 5%	0.87 ± 6%	6.0 ±10%
1800A	40.5 ± 5%	1.65 ± 6%	4.8 ±10%
1800B	41.0 ± 5%	1.25 ± 6%	4.8 ±10%

range between 15–30°C, a change of 5% in conductivity was measured.

The specific thermal constant c was determined using a simple calorimetric procedure with an accuracy of better than ±4%. For brain tissue-simulating liquids, c was determined to be 2.85 J/K/g ± 4% with a specific density (ρ) of 1.30 g/cm^3±1%. Comparison of these values for c with data from literature shows considerable agreement. Gucker *et al* measured 2.90 J/K/g for a similar aqueous sucrose solution [10]. The value for the brain tissue-simulating liquid that uses the sugar substitute Buthyldigol is 3.58 J/K/g (ρ = 0.98 g/cm^3 ± 1%).

C. Temperature Probe

The measurement of the local SAR by temperature probes has the advantage that small sensors with an active area below 1 mm^2 are readily available. Optical probes or thermistor probes with high resistive lines [11] provide the necessary field immunity. In the calibration process the limited temperature sensitivity of theses sensors can be overcome by applying high power.

In this study, a new nonmetallic temperature measurement system was used to measure the temperature increase. The probe is based on an NTC temperature sensor connected to four resistive lines [12]. The noise level of this system is about 100 times less than that of the two comparable optical devices on the market (±0.001°C averaged over 0.1 s; <±0.1 mK/s for 10 s exposure). The temperature increase in the liquid due to exposure to a 900 MHz field at two distances from the body is shown in Fig. 4. After every exposure period, the liquid was stirred until thermodynamic equilibrium was reached.

Thermodynamic dissipation processes are critical because of the large temperature gradients induced and were assessed by evaluating different time intervals. They were found to be negligible within the first 10 s for sugar–water solutions. The solution based on Buthyldigol had a considerably lower viscosity, so that the evaluation had to be reduced to an interval of 5 s.

A robot positioned the temperature probe in the liquid with an accuracy of better than ±0.2 mm. The disturbance caused by the probe holder has been shown to be negligible.

D. Results

The conversion factor γ was determined by comparing the values of the temperature probe and of the E-field probe on points along the line, which is normal to the Plexiglass bottom and above the dipole feedpoint (Fig. 3). These measurements were repeated at different power levels, at different distances of the RF source from the body, and at various frequencies (Figs. 5–8). The conversion factor was assessed by a least-square procedure considering all measured values. The results for the various tissues are summarized in Table I.

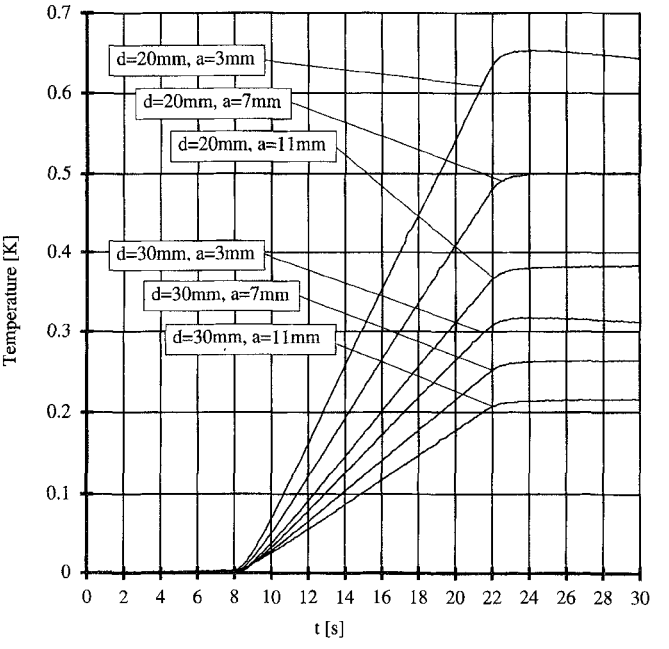

Fig. 4. Temperature increase measured during RF exposure to a 900-MHz field. The power input was 43 dBm. d = dipole distance from the simulating liquid: a = sensor distance from the acrylic glass bottom.

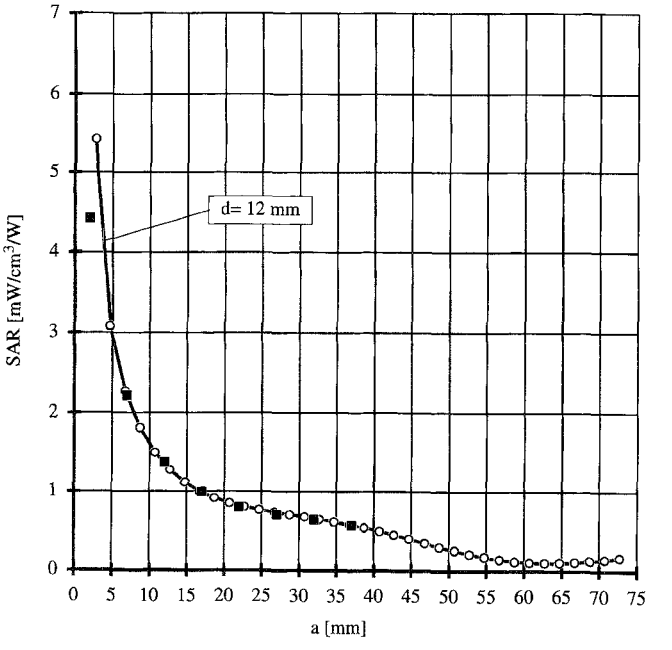

Fig. 5. SAR assessed by E-field (empty symbols) and temperature measurement (full symbols) at 450 MHz in brain-simulating liquid (ϵ_r = 47.0 and σ = 0.43 mho/m). The SAR was normalized to 1 W input power. Due to the inefficient coupling at 450 MHz, the closest possible distance of 12 mm between dipole and body was chosen. The conversion factor γ was determined to be 6.7 ± 10%.

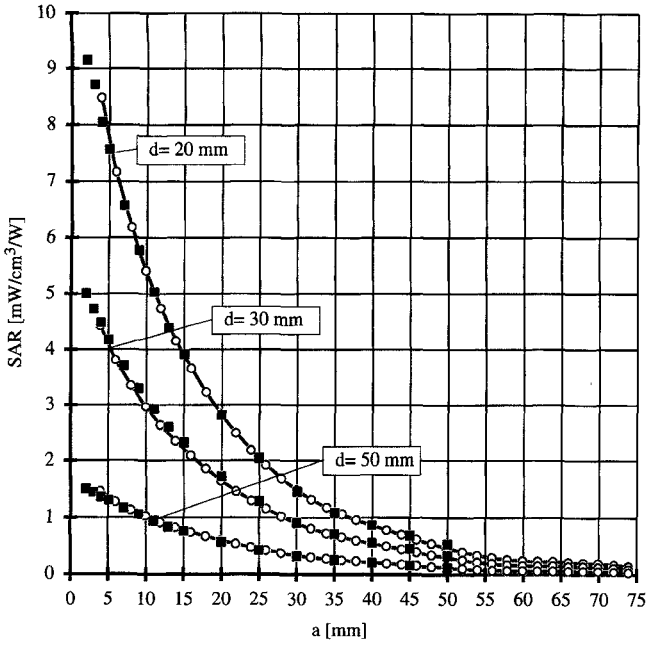

Fig 6. SAR assessed by E-field (empty symbols) and temperature measurement (full symbols) at 900 MHz in brain-simulating liquid ($\epsilon_r = 40.0$ and $\sigma = 0.87$ mho/m). The SAR was normalized to 1 W input power. The dipole distances from the body were 20, 30, and 50 mm. The conversion factor γ was determined to be 6.0 ± 10%.

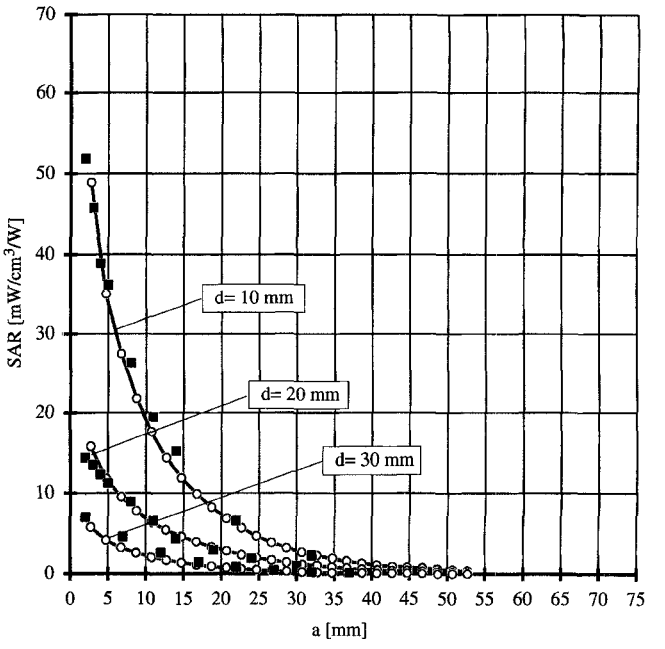

Fig. 8. SAR assessed by E-field (empty symbols) and temperature measurement (full symbols) at 1.8 GHz in brain-simulating liquid ($\epsilon_r = 41\ 0$ and $\sigma = 1.25$ mho/m). The SAR was normalized to 1 W input power. The dipole distances from the body were 10, 20, and 30 mm. The conversion factor γ was determined to be 4.8 ± 10%.

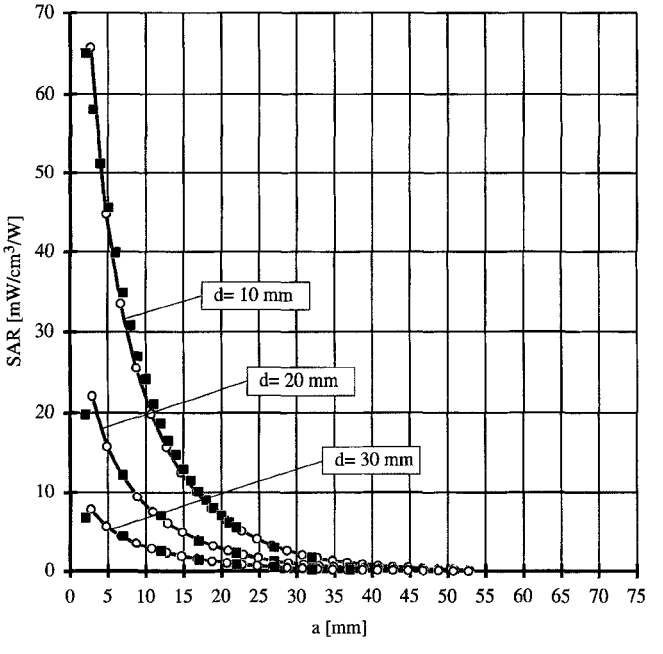

Fig. 7. SAR assessed by E-field (empty symbols) and temperature measurement (full symbols) at 1.8 GHz in brain-simulating liquid ($\epsilon_r = 40.5$ and $\sigma = 1.75$ mho/m). The SAR was normalized to 1 W input power. The dipole distances from the body were 10, 20, and 30 mm. The conversion factor γ was determined to be 4.8 ± 10%.

The accuracy of the conversion factor γ is mainly determined by the uncertainties in determining the correct electromagnetic and thermal properties of the tissue-simulating liquid. Using the "slot line" and "open coaxial" methods to determine the conductivity of the liquid results in an uncertainty of about ±6%. The specific heat of the liquid can be assessed to an accuracy of about ±4%. The E-field probe yields another ±5% and the temperature probe ±3%. Since these uncertainties and those of the positioning of the E-field probe (±1%) and of the temperature probe (±2%) as well as that of the power meters (±1%) can be considered to be statistically independent, the total uncertainty calculated based on root-mean-square is less than ±10%.

VI. Numerical Determination of Conversion Factor γ

To obtain a deeper insight into the behavior of the conversion factor, two numerical program packages based on two different techniques were used. This had the advantage of cross-validating the modeling and took advantage of the different strengths of each method.

The first technique applied was the three-dimensional (3-D) MMP software package. This is a frequency domain boundary technique suited for two–dimensional (2-D) and 3-D scattering problems within piecewise linear, homogeneous and isotropic domains. Details are given in [13] and [14].

The second software package, "MAFIA" is based on the finite integration technique (FIT). This technique is conceptually slightly different from the FDTD but results in the same numerical scheme. The open domains are bounded by second-order Mur absorbing boundary conditions. Details are given in [15] and [16].

A. Modeling of the Probe

To study the field distribution inside the probe depending on the electrical parameters of the surrounding media, different discretizations of the E-field probe were chosen. A transversal cut of the probe and a perspective view with the

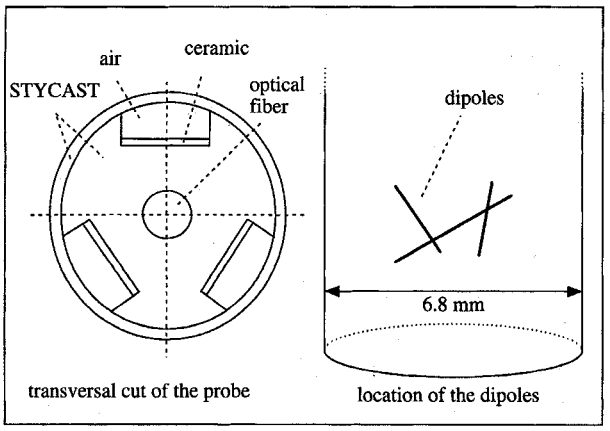

Fig. 9. Computer simulation model: Transversal cut of the probe and location of the dipoles.

location of the dipoles inside the probe is shown in Fig. 9. Different discretizations with increasing complexity have been compared:

1) The simplest numerical representation of the probe is a simple homogeneous, lossless cylinder 6.8 mm in diameter with the electrical properties of STYCAST 0005. The length of the cylinder is 15 mm, which has proven to be long enough to study the fields induced in the probe tip. MMP could only be used for this simple homogeneous model of the probe. The modeling with MMP required about 550 matching points at the boundary of the two domains and nine multipole expansions. As expected, the maximum errors (<10%) appeared on the matching points at the corners of the probe. In order to minimize these errors and to use a minimal number of expansion functions, the edge of the probe was slightly rounded. About 90 000 voxels were sufficient with MAFIA to model the whole computational domain of which about 5000 were used for the probe itself. Problems occurred at the outer boundaries when using open-boundary conditions and assuming the whole computational domain to be of a lossy material. The influence of possible reflected waves was assessed to be less than 3%.
2) A more complex model simulated the optical fiber in the center of the core. The fiber was discretized as a smaller homogeneous cylinder 1 mm in diameter with a relative permittivity of five in the center of the STYCAST cylinder.
3) Additional details were incorporated in a further model by the modeling of the three air holes (Fig. 9).
4) In the most complex model, three ceramic sheets on which the dipoles and lines are printed were simulated as well. This involved a discretization with 210 000 voxels, about 37 000 of which were needed for the probe itself.

The dipoles were not simulated in any of the models. The conversion factor can be calculated by integrating the electric field over the length of the dipoles (ds), first with biological tissue surrounding the structure and then with air surrounding

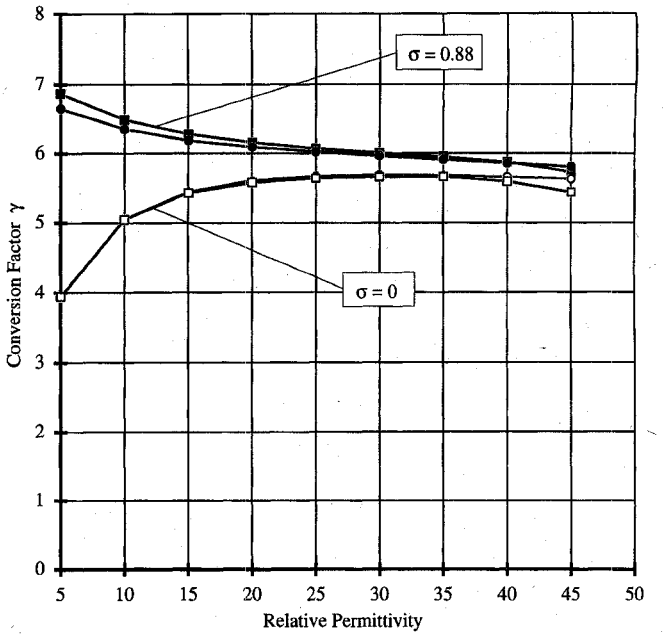

Fig. 10. Simulation: Conversion factor at 900 MHz as a function of the relative permittivity of the biological tissue. For absorbing biological tissue and nonabsorbing tissue. MAFIA modelings are displayed by squares, MMP modelings by circles.

it

$$\gamma = \frac{\sum_{i=1}^{3}\left[\int_{\text{Dipole}_i} \vec{E}\,\vec{ds}(\text{in tissue})\right]^2}{\sum_{i=1}^{3}\left[\int_{\text{Dipole}_i} \vec{E}\,\vec{ds}(\text{in air})\right]^2}. \tag{3}$$

This was performed for an incident plane wave, with the Poynting vector parallel to the probe axis and coming from the front. The E-field at the location of the dipole center in the absence of the probes was chosen to be 1 V/m in both cases.

B. Results of the Simulations

The simulations with the simple homogeneous models were performed for different dielectric properties of the probe's surrounding medium. Fig. 10 shows the dependence of the probe's conversion factor as a function of the relative permittivity. The frequency of the excitation was set to 900 MHz. These calculations were made for absorbing biological tissue and for nonabsorbing tissue.

The conductivity of the lossy material corresponds to the value used for the experimental investigations (0.88 mho/m, see below). The influence of the conductivity of the lossy material becomes less important for a larger real part of the complex permittivity. Within a wide range of relative permittivities (of biological tissue), the conversion factor or, in other words, the sensitivity of the probe changes by less than 10%. This is even true when changing the conductivity of the biological tissue within a certain range. For small real parts of the complex permittivity, however, the influence of the conductivity on the conversion factor is large. A comparison of the results of the two methods (MMP and MAFIA) reveals that

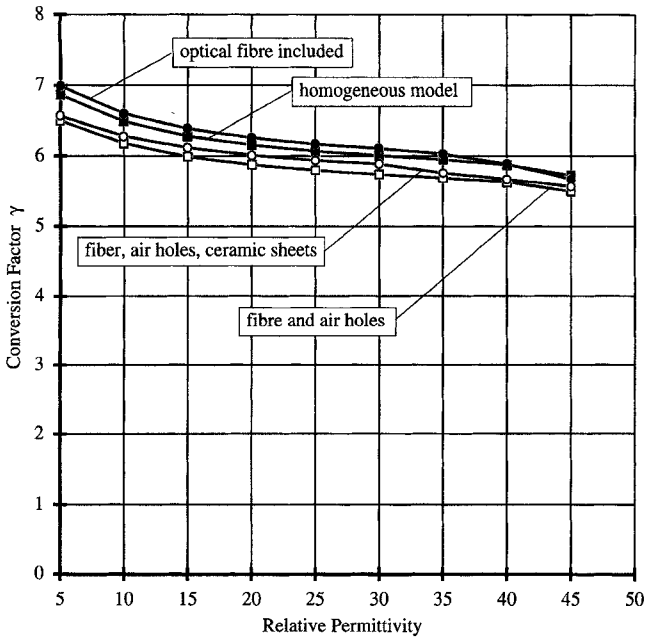

Fig. 11. Simulation: Conversion factor as a function of the relative permittivity of the biological tissue for different MAFIA models. The conductivity is 0.88 mho/m, the frequency 900 MHz.

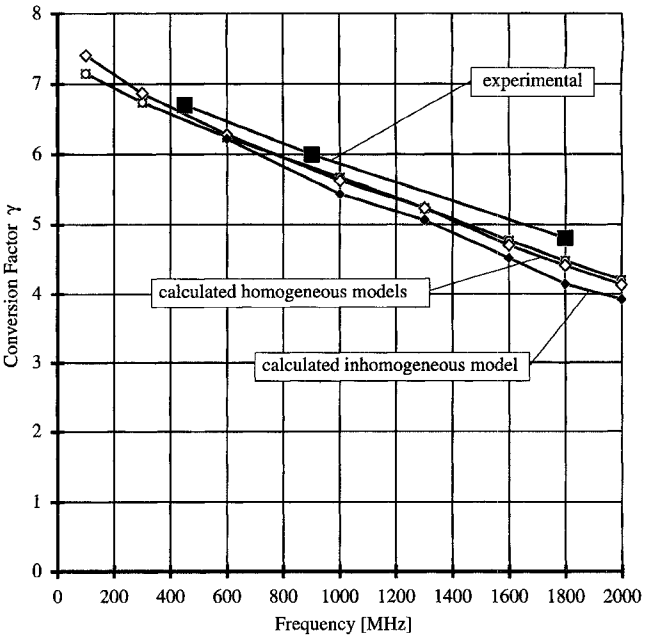

Fig. 12. Experimentally assessed conversion factor for brain tissue-simulating liquid in comparison with the values obtained from numerical simulation for homogeneous (empty symbols) and nonhomogeneous (filled symbols) modelings of the probe.

the difference is less than 1% for the nonabsorbing material and between 1–3% for the absorbing material.

In Fig. 11, the results for different MAFIA models are compared. The results of the homogeneous model are the same as discussed before. The conductivity was again chosen to be 0.88 mho/m and the frequency 900 MHz. The effect of the optical fiber inside the probe can be neglected.

For the more complex model with an optical fiber, ceramic sheets, and air holes, γ is about 6% lower than for the homogeneous model. Additional simulations that neglected the ceramic sheets or the air holes revealed that the air holes are responsible for the drop in the conversion factor.

In Fig. 12, the frequency dependence of γ is shown. The homogeneous models simulated with MMP and MAFIA are in close agreement with each other. Again, the values for the more complex modeling are slightly lower than those for the homogeneous modeling. In contrast to these findings, the experimentally determined conversion factors are larger than those of the simulations, which clearly demonstrates the limitations of this approach.

The reasons lie in the fact that any modeling involves many simplifications of the real probe, e.g., electrical parameters of the probe material were not measured, but were taken from the literature. The most important effect is most likely the change of the dipole capacitance, which depends on the surrounding media and could not be considered in the simulations. This effect, however, is expected to be more significant for probe designs in which the dipoles are positioned closer to the surrounding medium.

VII. Conclusion

A procedure has been presented which allows an absolute calibration for SAR measurements with an accuracy of better than ±10% for the described condition, which closely corresponds to that of the actual dosimetric assessments performed with the scanner described in [2]. Thus, further considerations with regard to polarization are not required. If such studies are needed, the techniques described can be used (see also [2]). Numerical techniques have proven to be adequate to assess the conversion factor γ if a precision of about ±20% is sufficient for this probe. For other probe designs, the uncertainties of the numerically determined conversion factors might be considerably larger.

Acknowledgment

The authors gratefully acknowledge the help of Mr. O. Egger, Ms. K. Poković, and Mr. J. de Keijzer for their support in this study.

References

[1] H. I. Bassen and G. S. Smith, "Electric field probes—A review," *IEEE Trans. Antennas Propagat.*, vol. 31, no. 5, pp. 710–718, Sept. 1983.
[2] T. Schmid, O. Egger, and N. Kuster, "Automated E-field scanning system for dosimetric assessments," *IEEE Trans. Microwave Theory Tech.*, vol. 44, pp. 105–113, Jan. 1996.
[3] T. Schmid and N. Kuster, "Novel E-field probes for close near field scanning," *IEEE Trans. Veh. Technol.*
[4] D. Hill, "Waveguide technique for the calibration of miniature implantable electric-field probes for use in microwave-bioeffects studies," *IEEE Trans. Microwave Theory Tech.*, vol. 30, pp. 92–99, Jan. 1982.
[5] K. Meier and N. Kuster, "Dosimetric measurements on various GSM-mobile telephones," in *Proc. 17th Ann. Meet. Bioelectromagnetics Soc.*, Boston, June 18–22, 1995, p. 30.
[6] N. Kuster and Q. Balzano, "Energy absorption mechanism by biological bodies in the near field of dipole antennas above 300 MHz," *IEEE Trans. Veh. Technol.*, vol. 41, no. 1, pp. 17–23, Feb. 1992.
[7] C. Gabriel, personal communication.
[8] P. Pethig, "Dielectric properties of biological materials: Biophysical and medical applications," *IEEE Trans. Elect. Insulation*, vol. 19, no. 5, pp. 453–474, 1984.

[9] G. Hartsgrove, A. Kraszewski, and A. Surowiec, "Simulated biological materials for electromagnetic radiation absorption studies," *Bioelectromagnetics,* vol. 8, no. 1, pp. 29–36, Jan. 1987.
[10] F. T. Gucker and F. D. Ayres, "The specific heats of aqueous sucrose solutions," *Am. J. Chem.,* vol. 59, pp. 447–452, Mar. 1937.
[11] M. Burkhardt, K. Pokovic, M. Gnos, T. Schmid, and N. Kuster, "Numerical and experimental dosimetry of petri dish exposure setups," *J. Bioelectromagnetic Soc.,* in press.
[12] R. R. Bowman, "A probe for measuring temperature in radio-frequency-heated material," *IEEE Trans. Microwave Theory Tech.,* vol. 24, no. 1, pp. 43–45, 1976.
[13] C. Hafner and L. H. Bomholt, *The 3D Electrodynamic Wave Simulator.* New York: Wiley, 1993.
[14] N. Kuster, "Multiple multipole method for simulating EM problems involving biological bodies," *IEEE Trans. Biomed. Eng.,* vol. 40, no. 7, pp. 611–620, July 1993.
[15] T. Weiland, "Maxwell's grid equations," *Frequenz,* vol. 44, no. 1, pp. 9–16, 1990.
[16] CST, *The MAFIA Collaboration, User's Guide Mafia Version 3.x.* CST GmbH, D 64289 Darmstadt, Germany, 1994.

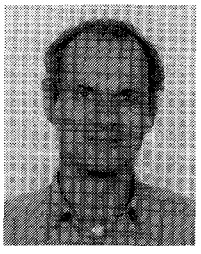

Klaus Meier was born in Austria in March 1965. He received the Diploma Degree in electrical engineering from the Swiss Federal Institute of Technology (ETH) Zurich in 1991.

He joined the Institute for Field Theory and Microwave Electronics at the ETH in 1991. Since 1992, he has been involved in the development of the dosimetric assessment system DASY. He is currently finishing his Ph.D. on the development of a phantom for standardized compliance tests of mobile telecommunication equipment. He is a cofounder of the spin-off company Schmid & Partner Engineering AG.

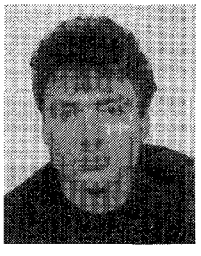

Michael Burkhardt was born in Germany in March 1969. He received the Diploma in electrical engineering from the Technische Hochschule Darmstadt in 1995 with emphasis on computational electrodynamics. In 1993, he conducted his semester work at the Institut National Polytechnique de Grenoble (INPG), France.

In May 1995, he joined the Institute of Field Theory and Microwave Electronics, ETH, where he is involved in the development of a modular platform for electromagnetic simulations. In addition, he has performed various studies using time and frequency domain techniques.

Thomas Schmid worked from 1984 to 1987 at the Swiss Federal Institute of Technology in Zurich. He was involved in research into medical applications of microwave and electroacoustic wave propagation in crystals. From 1988 to 1992, he worked for OIM (Organizacion Intergubernamental de Migraciones, Geneva), where he was involved in technical and educational development projects for Central America. During this time, he served as Professor at the Universidad National de Ingenieria (UNI) in Managua, Nicaragua and founded as an independent enterprise a service-center (UNITRON) at the University for State Institutions and Industries. In 1990, he was responsible for the technical setup of the general elections in Nicaragua. In 1993, he joined the Laboratory for Electromagnetic Fields and Microwave Electronics, ETH, where he has been developing near-field probes and the dosimetric assessment system DASY. In late 1994, he cofounded the spin-off company Schmid & Partner Engineering AG.

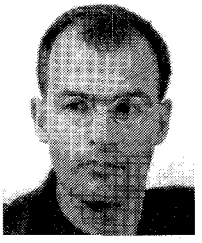

Niels Kuster was born in Olten, Switzerland in June 1957. He received the Diploma and Ph.D. degrees in electrical engineering from the Swiss Federal Institute of Technology (ETH) in Zurich.

He joined the Electromagnetics Laboratory at ETH in 1985, where he was involved in the research and development of the Generalized Multipole Technique (GMT) and the 3D MMP code. In 1992, he was invited Professor at Motorola Inc. in Fort Lauderdale, FL for a trimester. He currently is Professor at the Department of Electrical Engineering, ETH Zurich. His research interests include all aspects of numerical methods in electrodynamics, antenna design, and bioelectromagnetics.

Dr. Kuster is a member of various scientific societies and official member of URSI Commission K.